energies

MDPI

Article

A Dynamic Investigation of a Solar Absorption Plant with Nanofluids for Air-Conditioning of an Office Building in a Mild Climate Zone

Luca Cirillo [1], Sabrina Gargiulo [1], Adriana Greco [1], Claudia Masselli [1,*], Sergio Nardini [2], Vincenzo Orabona [1] and Lucrezia Verneau [1]

[1] Department of Industrial Engineering, Università degli Studi di Napoli "Federico II", Piazzale Tecchio 80, 81031 Napoli, Italy; luca.cirillo2@unina.it (L.C.); adriana.greco@unina.it (A.G.)
[2] Department of Engineering, DI, Università degli Studi della Campania "L. Vanvitelli", Via Roma 29, 81031 Aversa, Italy; sergio.nardini@unicampania.it
* Correspondence: claudia.masselli@unina.it

Abstract

This study explores the impact of using water-Al_2O_3 nanofluids, at different nanoparticle concentrations, in solar thermal collectors for solar cooling applications. Improving the seasonal energy performance of solar cooling systems is a current research priority, and this work investigates whether nanofluids can significantly enhance system efficiency compared to traditional heat transfer fluids. A transient simulation was carried out using a dynamic model developed in TRNSYS (TRANsient SYstem Simulation), evaluating the system performance throughout the cooling season. The results show that in July, under low volumetric flow conditions and with nanoparticle concentrations of 0.6% and 0.3%, the solar fraction reaches a maximum value of 1. Using a nanofluid at 0.6% concentration leads to significantly higher fractional energy savings compared to pure water. Despite increased pumping energy, the overall energy savings—which include the contribution from an auxiliary boiler—exceed 80% when nanofluids are used. This study goes beyond previous work by providing a dynamic, system-level simulation of nanofluid-enhanced solar cooling performance under realistic operating conditions. The findings demonstrate the practical potential of nanofluids as a valid and more energy-efficient alternative in solar thermal applications.

Keywords: nanofluids; solar energy; thermal efficiency; solar cooling; TRNSYS

Academic Editor: Marco Marengo

Received: 6 June 2025
Revised: 25 June 2025
Accepted: 27 June 2025
Published: 1 July 2025

Citation: Cirillo, L.; Gargiulo, S.; Greco, A.; Masselli, C.; Nardini, S.; Orabona, V.; Verneau, L. A Dynamic Investigation of a Solar Absorption Plant with Nanofluids for Air-Conditioning of an Office Building in a Mild Climate Zone. *Energies* **2025**, *18*, 3480. https://doi.org/10.3390/en18133480

1. Introduction

In recent decades, the growing need for efficient cooling technologies—ranging from electronics to air-conditioning systems—has intensified the search for advanced heat transfer fluids. Conventional fluids such as air, water, and ethylene glycol exhibit relatively low thermal conductivity, which limits their application in high-performance thermal systems. Earlier attempts to enhance thermal performance involved suspending millimeter- or micrometer-sized solid particles in liquids [1]. However, these suspensions led to particle sedimentation, abrasion, and clogging, and required high particle concentrations to be effective. The advent of nanotechnology allowed the development of nanofluids (NFs), defined as colloidal suspensions of nanoparticles (typically < 100 nm) in conventional base fluids. Due to their large surface area and enhanced Brownian motion, nanofluids exhibit improved thermal conductivity and heat transfer performance compared to both

the base fluid and traditional slurries. Choi first coined the term "nanofluid" in 1993 [2], and subsequent studies confirmed that nanofluids offer superior thermal characteristics with acceptable stability [3,4]. The thermo-physical properties of nanofluids depend on nanoparticle type, shape, and concentration, and the choice of base fluid. For example, ref. [3] highlighted the role of surfactants in stabilizing carbon nanotube-based nanofluids, showing that oleic acid derivatives enhanced stability, while non-ionic surfactants improved thermal conductivity. Ref. [4] demonstrated that mixing water and ethylene glycol with metal-oxide nanocomposites significantly enhanced conductivity, although viscosity and density also increased with concentration. These findings have motivated the exploration of nanofluids in a variety of thermal applications, including PV/T systems [5–8], battery cooling [9], and even nuclear reactors [10,11]. Among available nanoparticles, alumina (Al_2O_3) is one of the most studied due to its good thermal properties, stability, low cost, and environmental compatibility [12,13]. Numerous studies have investigated the use of Al_2O_3–water nanofluids in flat plate and evacuated tube collectors, reporting improvements in collector thermal efficiency up to 15–20% [14–18]. For instance, Hawwash et al. [19] found a thermal efficiency gain between 3% and 18% with Al_2O_3 concentrations up to 0.5%, although excessive concentrations could lead to higher pressure drop. Other works, such as [17], examined how varying flow rates and nanoparticle concentrations affect the outlet temperature and collector performance. Solar Cooling Systems (SCSs) represent a strategic application for integrating renewable energy with nanofluids [20,21]. These systems can help meet the high cooling demands in summer months while reducing greenhouse gas emissions and dependency on fossil fuels. Reviews such as [22,23] have discussed the potential of nanofluids in solar thermal applications and their environmental and economic implications. However, most of the existing literature either focuses on steady-state analyses or lacks detail on real-case dynamic behavior. This study investigates the dynamic behavior of a solar-assisted single-effect absorption cooling system using Al_2O_3–water nanofluids as working fluid within the solar collector loop. The system is designed to meet the cooling demand of a real office building located in Naples, Italy—a representative site in a mild Mediterranean climate. The simulation is carried out using TRNSYS, and includes the modeling of collectors, storage tanks, auxiliary boiler, chiller, and fan coils. Three volumetric flow rates (0.24, 0.47, and 0.71 L/s) and two nanoparticle concentrations (0.3% and 0.6%) are analyzed, and the results are compared with a baseline case using pure water. Key performance indicators such as Solar Fraction (SF), Primary Energy Savings (f), and pumping energy are evaluated over the entire cooling season (June–September).

Several previous works have investigated the application of solar-assisted absorption systems for space cooling using dynamic simulation tools. In particular, in our earlier studies [24,25], TRNSYS-based models were employed to evaluate the performance of solar cooling systems operating with conventional and nanofluid-based working fluids. While those studies provided valuable insights into seasonal energy performance and system behavior, they were based on simplified system-level simulations with limited spatial and thermal resolution. The present work proposes a model that allows for the evaluation of dynamic operating conditions under realistic boundary profiles, improving the accuracy and applicability of the simulation results. Compared to the previous TRNSYS-based studies, the current model offers enhanced predictive capabilities and opens new perspectives for system optimization and design refinement.

The novelty of this work lies in the following:

- Exclusive use of nanofluids in the solar loop with detailed thermo-physical modeling.
- Dynamic, hourly simulation in TRNSYS over the summer period.
- Sensitivity analysis on flow rate and concentration effects.
- Assessment of pumping energy penalty, often overlooked in the literature.

2. System Configuration

The SCS configuration depicted in Figure 1 has been specifically built to meet the cooling needs of an office building located in Naples. The thermal component of the system comprises evacuated tube collectors (ETCs), a hot storage tank (HST), a circulation pump, and a controller to facilitate heat transfer.

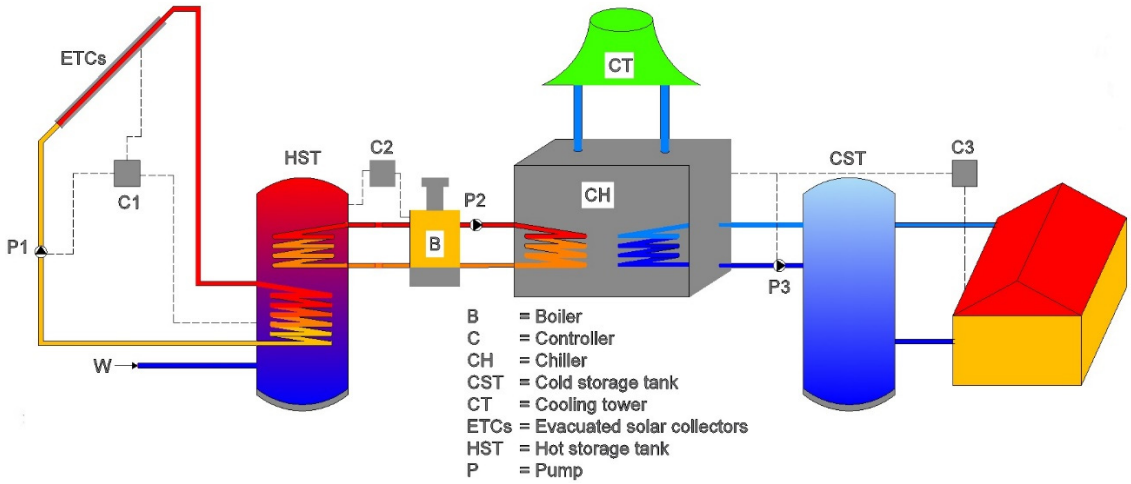

Figure 1. Schematic layout of the simulated solar cooling system. The configuration includes evacuated tube collectors, a hot storage tank, an auxiliary boiler, and a single-effect absorption chiller connected to fan coils.

The fluid within the collectors is heated by solar radiation and subsequently transferred to a high-temperature storage tank at $T_{coll,o}$. If the temperature of the outlet water from the storage tank ($T_{st,o}$) falls below 90 °C, the working fluid is returned to the collectors through pumping. The ETCs and chiller are maintained in a distinct manner, with the hot loop being sustained until the storage tank attains the appropriate temperature. The auxiliary fluid utilized in the hot loop (from the solar collector to hot storage tank) of this specific investigation is a nanofluid consisting of water and alumina nanoparticles.

Table 1 presents the physical properties of the alumina nanoparticles and clean water employed in the study.

Table 1. Physical properties of nanomaterial and water.

Material	ρ (kg/m^3)	k (W/mK)	c_p (J/kgK)	μ (Pa s)	Ref.
Al_2O_3	3970	36	773		[26]
Water	997	0.60	4178	$8.94 \cdot 10^{-4}$	-
Water–Al_2O_3 (vol. 0.3%)	1010	0.62	4121	$9.01 \cdot 10^{-4}$	[27]
Water–Al_2O_3 (vol. 0.6%)	1025	0.64	4066	$9.01 \cdot 10^{-4}$	[27]

The nanofluid consists of two separate substances that retain their characteristic properties (conductivity, specific heat, and density). While retaining their characteristic properties, the substances that make up the nanofluid give rise to a homogeneous mixture that has uniform physical properties throughout the sample.

The thermal conductivity of nanofluids is evaluated by the following equation [28]:

$$\frac{k_{nf}}{k_{bf}} = \frac{\frac{k_p}{k_{bf}} + 5 - 5\left(1 - \frac{k_p}{k_{bf}}\right)\phi}{\frac{k_p}{k_{bf}} + 5 + \left(1 - \frac{k_p}{k_{bf}}\right)\phi} \quad (1)$$

where k_{nf} is the thermal conductivity of the nanofluid, k_{bf} and k_p are the thermal conductivity of the base fluid and nanoparticle, respectively, ϕ is the volume fraction of the nanoparticles (%). Various equations can be used to determine the specific heat capacity of a nanofluid, but the most precise formula is the one proposed by Xuan and Roetzel [26]:

$$c_{pnf} = \frac{\phi\rho_p c_{pp} + (1-\phi)\rho_{bf} c_{pbf}}{\rho_{nf}} \quad (2)$$

where c_{pnf} and c_{pbf} are the heat capacity of the nanofluid and base fluid, respectively, c_{pp} is the heat capacity of the nanoparticle.

The density is evaluated by means (Kasaeian et al. [28]):

$$\rho_{nf} = \rho_p\phi - \rho_{bf}(1-\phi) \quad (3)$$

where ρ_{nf} and ρ_{bf} are the density of the nanofluid and base fluid, respectively, ρ_p is the density of the nanoparticle. Einstein's equation [29] can be used for calculating the dynamic viscosity of the nanofluid:

$$\mu_{nf} = (1 + 2.5\phi)\mu_{bf} \quad (4)$$

where μ_{nf} and μ_{bf} are the dynamic viscosity of the nanofluid and base fluid, respectively.

The absorption chiller operates on a single-effect system and obtains its hot fluid supply from a hot storage tank (HST) with a setpoint temperature of 90 °C. If the temperature of the HST, denoted as $T_{st,o}$, falls below the predetermined setpoint, a secondary boiler is triggered to maintain the desired temperature of the hot water entering the chiller. This is particularly important during periods characterized by low or absent solar radiation. Hence, a thermostat is employed to regulate the temperature of the fluid entering the chiller on the intake. Furthermore, the chiller is linked to a cooling storage tank (CST), which functions as a reservoir of energy for the fan coils (FC) and a cooling tower (CT).

3. Modeling in TRNSYS

The solar system described in this study is modeled with weather data from Naples (40°51′22″ N; 14°14′47″ E), using a 17.5 kW single-effect absorption chiller. The simulation has the following assumption:

- The simulation does not take into account the outcomes of the boiling of the auxiliary fluid;
- The analysis does not take into account the decreases in pressure that arise within the pipes and valves. Therefore, the predicted performance values may be higher than those in a real system.

The solar cooling system's layout in TRNSYS is illustrated in Figure 2. In Macro-2 there are settings data related to lighting, environmental data, and real time display of temperatures.

3.1. Solar Collector

This study focuses on ETCs and examines the impact of using water with varying amounts of nanoparticles concentrations of Al_2O_3 (0%, 0.3%, and 0.6%) as the fluid. The study also investigates three different volumetric flow rates (0.24 L/s, 0.47 L/s, and 0.71 L/s) of the fluid. The equations presented in Table 2, which were previously defined by Ghaderian and Sidik [27] in their experimental investigation of the effects of Al_2O_3–distilled water nanofluid on the thermal efficiency of a solar collector, are utilized in this study. The Δt and G are the temperature difference across the solar collector and the solar irradiance, respectively.

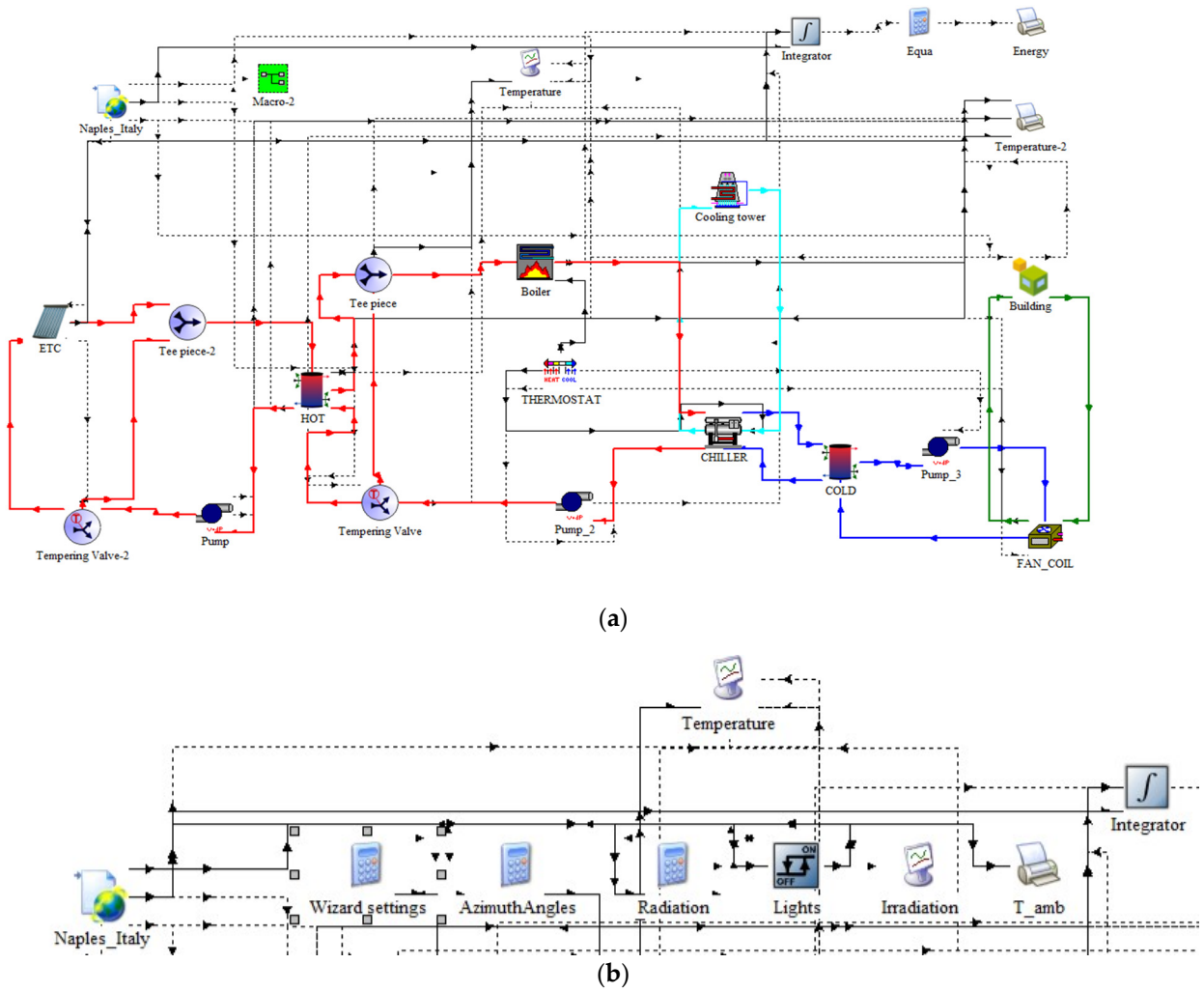

Figure 2. TRNSYS model: (**a**) system plant; (**b**) scheme of Macro-2. This configuration represents the implementation of the solar cooling system in TRNSYS, including collector loops, storage tanks, and absorption chiller subsystems.

Table 2. Efficiency data from the experimental results of Ghaderian and Sidik [27].

Working Fluid	$\dot{V}$ [L s^{-1}]	Nanoparticles	Vol. %	Equation
(Al_2O_3/DW)	0.24	Al_2O_3	0.3	$\eta = 0.3652 - 0.7351\frac{\Delta T}{G}$
(Al_2O_3/DW)	0.47	Al_2O_3	0.3	$\eta = 0.4477 - 1.7180\frac{\Delta T}{G}$
(Al_2O_3/DW)	0.71	Al_2O_3	0.3	$\eta = 0.4782 - 1.8417\frac{\Delta T}{G}$
(Al_2O_3/DW)	0.24	Al_2O_3	0.6	$\eta = 0.4450 - 0.7404\frac{\Delta T}{G}$
(Al_2O_3/DW)	0.47	Al_2O_3	0.6	$\eta = 0.5697 - 2.0186\frac{\Delta T}{G}$
(Al_2O_3/DW)	0.71	Al_2O_3	0.6	$\eta = 0.5891 - 2.3734\frac{\Delta T}{G}$
Water	0.24	-	-	$\eta = 0.1958 - 0.7344\frac{\Delta T}{G}$
Water	0.47	-	-	$\eta = 0.2412 - 1.3648\frac{\Delta T}{G}$
Water	0.71	-	-	$\eta = 0.3234 - 1.4744\frac{\Delta T}{G}$

In this work, the same solar collector is considered but with a total absorbing area of 100 m^2 and the specifications of the solar collector represented in Table 3.

Table 3. Specifications of the ETC.

Specification	Unit	Dimension
Gross area	m^2	2.57
Aperture area	m^2	2.22
Absorber area	m^2	2.36
Length	m	1.80
Width/width incl. connection	mm	1560/1612
Max operating pressure	bar	10
Absorber	-	Aluminum
Absorption (α)/emission (ε)	-	0.96/0.06
Collector housing	-	Aluminum
Collector glazing	-	Evacuated tubes
Number of tubes	-	18
Outer glass tube diameter	mm	6
Inner glass tube diameter	mm	5
Sealing material	-	Silicone
Frame material	-	Stainless steel

3.2. Storage Tank

Based on the design of the solar field, a filling factor of approximately 40 L/m^2 is considered, resulting in a total volume of about 4000 L. Therefore, a 5000 L hot storage tank (HST) was selected to ensure effective heat exchange and system autonomy during periods of low solar radiation. This sizing aligns with findings from previous studies, such as [30], where an optimal storage volume of about 40 L/m^2 was determined for similar systems. As for the thermal storage of the cold circuit, it was decided to use a cold storage tank (CST) of 2000 L since there are 20 fan coils inside the building that require approximately 1000 L of water to deliver the right cooling power, and also, in this case, to achieve continuity of the cycle, it was decided to increase the volume of the storage tank in order for it to be used as a thermal flywheel.

A stratified storage tank with consistent losses is employed, and the multi-node approach is put into action by dividing the tank into N nodes. The tank governs the energy balance of each node over time. The chiller receives water from the highest node of the tank and feeds it back into the lower node of the tank. The HST is partitioned into six partitions, while the CST has only one node. When the fluid temperature drops below the designated temperature, the auxiliary boiler (Type 122) activates. When the boiler is on, the heat energy required, $\dot{Q}_{\text{boiler}}$, to increase the temperature of the working fluid from the inlet temperature, $T_{st,in}$, to the desired outlet temperature, $T_{st,o}$, is calculated as:

$$\dot{Q}_{boiler} = \dot{m}_w c_{p,w} (T_{st,o} - T_{st,in}) \quad (5)$$

where $\dot{m}_w$ and $c_{p,w}$ is the mass flow rate and specific heat of water, respectively.

3.3. Absorption Chiller

A HST provides hot water to the absorption chiller, which then uses it to regenerate the absorbed refrigerant in the generator from the refrigerant–absorbent mixture. The absorption chiller has a cooling capacity of 17.5 kW and a rated COP of 0.71; this equipment operates according to [31].

Upon establishing the activation of the absorption chiller via the control signal value, The Type 107 chiller initially computes the proportion of the design load at which it needs to function. This computation entails determining the quantity of energy required to be

extracted from the chilled water stream to adjust it from its initial temperature to the desired setpoint temperature:

$$\dot{Q}_{removed} = \dot{m}_{chilled\_w} c_{p,chilled\_w} (T_{chilled\_w} - T_{chilled\_set}) \quad (6)$$

The $T_{chilled\_set}$ is the setpoint of the supply cold water, equal to 7 °C. The required energy removal is then divided by the machine's capacity to determine the fraction of design load at which the machine is required to operate.

$$f_{design} = \frac{\dot{Q}_{removed}}{Capacity_{rated}} \quad (7)$$

where the $Capacity_{rated}$ is equal to 17.5 kW. When functioning at its maximum capacity, the chiller necessitates the designated energy input to operate effectively. Conversely, during partial load operation, only a portion of the designated energy input is needed.

The hot water stream outlet temperature is then:

$$T_{out,chiller} = T_{in,chiller} - \frac{\dot{Q}_{removed}}{\dot{m}_w \cdot cp_w} \quad (8)$$

3.4. Building Loads

The solar cooling system was created to fulfill the cooling needs of a 250-square-meter office building with 37 m^2 of windows, which accounts for roughly 15% of the dispersing surface (Figure 3). The building operates from 8:00 a.m. to 4:00 p.m. and is considered one thermal zone.

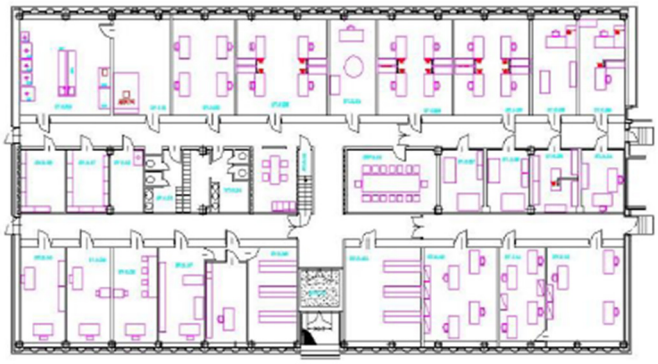

Figure 3. Map of the office building. The simulation model was constructed based on this layout, including internal zones and window distribution.

The daily cooling load profile is primarily driven by internal heat gains due to occupancy, equipment, and lighting, as well as by solar radiation entering through windows. The load begins to increase after 8:00 a.m., reaches its peak between 12:00 and 2:00 p.m., and gradually decreases until the end of the operating hours at 4:00 p.m. This behavior reflects typical office use patterns and has been modeled accordingly in TRNSYS using hourly schedules for internal gains and occupancy. The model assumes a gradual buildup of heat during the morning, with a declining phase in the afternoon as solar radiation intensity decreases and internal sources are switched off. This trend is also reflected in the monthly cooling demand shown in Figure 4a, where higher energy requirements are observed in July and August, consistent with peak solar radiation and occupancy-related internal loads.

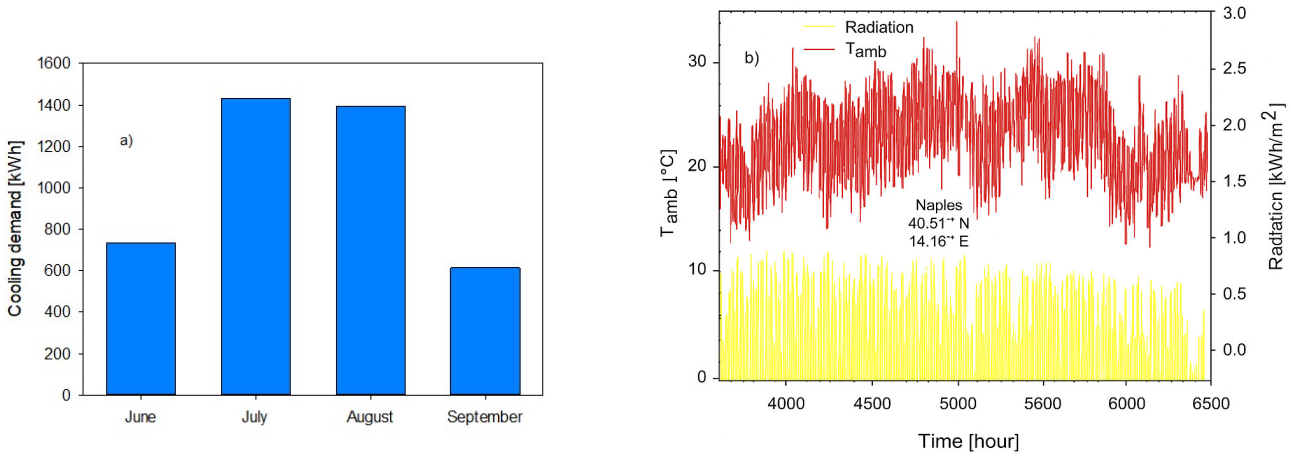

Figure 4. Working conditions: (**a**) monthly cooling demand considering heat gains; (**b**) hourly solar radiation and ambient temperature profiles over the year. The data highlights the seasonal variation in solar availability and the thermal context in which the system operates.

A 3D model of the building was constructed using a graphical tool (SketchUp) that was imported into TRNSYS. This model included information on occupancy patterns, as well as the physical properties of the structures—Table 4.

Table 4. Physical properties of building components.

Component	Thickness [cm]	Mass [kg/m^2]	Thermal Trasmittance [W/(m^{2}K)]
External wall	33	370	1.26
Ceiling	35	506	1.25
Floor	35	506	1.25
Window (double glass)—Argon gas	1.2	-	2.072
Aluminum frame	-	-	2.405

By simulating the building model, a typical hourly cooling demand for each season was generated. The monthly cooling energy demand values are displayed in Figure 4a. The cooling demand of the building was estimated based on geometrical modeling in SketchUp and standardized internal load profiles, given the absence of real measurement data. Occupancy, lighting, and equipment schedules were assigned using typical values for small office buildings in Southern Europe.

3.5. Weather Data

The weather data used pertains to Naples, with a latitude and longitude of 40.51° N and 14.16° E, respectively. The climatic data used for the dynamic simulation were obtained from a Typical Meteorological Year (TMY2) dataset for Naples, provided by the National Solar Radiation Data Base (NSRDB) of the U.S. Department of Energy. The changes in ambient temperature and solar radiation over the course of a year are displayed in Figure 4b.

During the summer months, the highest temperatures range from 30–35 °C. The system components are outlined in Table 5.

Table 5. Operating parameters used in TRNSYS modelling.

Component	Description
Hot water absorption chiller (Type 107)	
Peak cooling load	17.5 kW
COP	0.71
Chilled water setpoint temperature	0.667
Minimum operative temperature	90 °C
Specific heat of hot water, cooling water and chilled water	4.18 kJ kg^{-1} K^{-1}
Evacuated tube solar collectors (ETCs—Type 71)	
Collector area	100 m^2
Number in series	1
Efficiency mode (Inlet temperature)	1
Collector efficiency	Table 2
Solar collector slope	40°
Pump (Type 740)	
Hot water flowrate between hot storage tank and ETCs	0.24/0.47/0.71 L s^{-1}
Specific heat of fluid (water)	4.18 kJ kg^{-1} K^{-1}
Specific heat of fluid (0.3% vol.)	3.81 kJ kg^{-1} K^{-1}
Specific heat of fluid (0.6% vol.)	3.50 kJ kg^{-1} K^{-1}
Fluid density (water)	1000 kg m^{-3}
Fluid density (0.3% vol.)	1087.45 kg m^{-3}
Fluid density (0.6% vol.)	1176.60 kg m^{-3}
Pump_2 (Type 740)	
Hot water flowrate between hot storage tank and chiller	0.5 L s^{-1}
Specific heat of fluid (water)	4.18 kJ kg^{-1} K^{-1}
Fluid density (water)	1000 kg m^{-3}
Hot storage tank (Type 4a)	
Tank type	Stratified
Tank loss coefficient	0.694 W m^{-2} K
Volume	5 m^3
Fluid density (water)	1000 kg m^{-3}
No. nodes	6
Supplementary boiler (Type 122)	
Setpoint temperature	90 °C
Maximum heating rate	24 kW
Deadband for heating	5°C (ΔT)
Cold storage tank (Type 4a)	
Tank type	Stratified
Tank loss coefficient	0.694 W m^{-2} K
Volume	2 m^3
Fluid density (water)	1000 kg m^{-3}
No. nodes	1
Cooling Tower (Type 510a)	
Rated Fan Power	1.36 kW
Fluid specific heat	4.19 kJ/(kg K)
Time step of the simulation	1 h
Duration of the simulation	1 June–30 September

3.6. Uncertainty Analysis

To assess the impact of key input parameters on the system's performance, a deterministic sensitivity analysis was conducted. Four critical parameters—solar irradiance, nanofluid viscosity, collector efficiency, and storage tank heat loss coefficient—were individually varied by ±10% around their nominal values. For the purpose of the sensitivity analysis within the dynamic simulation framework, the variation of each input parameter was applied as a global ±10% scaling factor to its time-dependent profile (e.g., hourly solar radiation or fluid viscosity over time). This allows us to estimate the influence of each variable on cumulative seasonal performance indicators such as SF. The resulting changes in the solar fraction were analyzed, and the relative sensitivity index was computed. The analysis revealed that solar irradiance and nanofluid viscosity have the most significant influence on the system's performance, as detailed in Table 6. The resulting variation in solar fraction (SF) was calculated and used to compute the relative sensitivity index:

$$S = \frac{\Delta SF}{\Delta x} \cdot \frac{x}{SF} \tag{9}$$

where x represents the value of the parameter varied. Similar studies, such as Shirazi et al. [32], have applied multi-objective simulations to quantify the propagation of input uncertainties and assess their impact on solar-assisted cooling system performance modeled in TRNSYS.

Table 6. Sensitivity analysis of key input parameters on the seasonal solar fraction.

Parameter	Nominal Value	Variation ±10%	ΔSF (%)	Relative Sensibility (S)
Solar radiation	800 W/m^2	720–880 W/m^2	±6%	0.75
Nanofluid viscosity (range 30–90 °C)	0.9 mPa·s	0.81–0.99 mPa·s	±4.2%	0.52
Collector efficiency (seasonal)	0.70	0.63–0.77	±3.5%	0.45
Heat loss Storage Tank	1.0 W/(m^2 K)	0.9–1.1 W/(m^2 K)	±1.8%	0.22

4. Performance Factors

In order to evaluate the performance of the system with different working fluids, the solar fraction (SF) and primary energy savings (f) are introduced:

4.1. Solar Fraction

The solar fraction refers to the proportion of a plant's energy needs that are met by a solar system. This value can range from 0 to 1, where 0 means that the boiler provides all of the energy required and 1 means that the solar collectors fully power the system. The objective of an SCS is to achieve an SF value close to 1. The formula for calculating solar fraction is provided in reference [33]:

$$SF = Q_{solar} / (Q_{solar} + Q_{boiler}) \tag{10}$$

where Q_{solar} is the monthly solar thermal gain from solar collectors, and Q_{boiler} is the heat of the auxiliary boiler.

4.2. Primary Energy Savings

Primary energy savings refers to the reduction in the consumption of primary energy resources resulting from the implementation of energy-efficient measures or technologies. This term encompasses the conservation of energy at the source, such as reducing the amount of fossil fuels or other primary energy sources required to produce electricity, heat, or other forms of energy. Primary energy savings measures aim to minimize energy

waste, promote sustainability, and mitigate environmental impacts associated with energy production and consumption. The primary energy savings is defined by following equation [34]:

$$f = 1 - \left[\frac{\frac{Q_{boiler}}{\varepsilon_{heat}}}{\frac{Q_{cooling,ref}}{COP_{ref}\varepsilon_{electricity}}} \right] \quad (11)$$

The expression includes several terms: ε_{heat}, which denotes the efficiency of the boiler; $Q_{cooling,ref}$, which represents the cooling energy delivered by a standard refrigeration system; COP, which stands for the coefficient of performance of the compression chiller; and $\varepsilon_{electricity}$, which represents the ratio of electricity produced to the primary fossil energy. The square brackets contain a ratio that compares the primary energy consumption of the auxiliary boiler in the SCS to the total primary energy consumption of a conventional refrigeration system that would provide the same cooling output. Typical values of the conversion factors are the following, according to [34]:

$$\varepsilon_{electricity} = 0.4$$
$$\varepsilon_{heat} = 0.78$$
$$COP = 3.5$$

5. Results and Discussion

The entire summer period, spanning from June to September, was simulated using a 1-h interval in the TRNSYS simulation. Despite peak summer temperatures exceeding 32 °C, the chosen system effectively kept the room temperature near the desired 26 °C. The paper extensively examines the operation of this system, which utilizes nanofluids as the working fluid to enhance the efficiency of the solar collector and power a heat absorber for cooling purposes. Various parameters are investigated, such as nanofluid concentration, operating temperature, and cooling cycle efficiency, to optimize the overall system performance. The objective is to identify the optimal operating conditions to maximize energy efficiency and the cooling system's performance.

5.1. Temperatures

The temperature trends on a typical summer day are illustrated in Figure 5. The TRNSYS model includes heat losses from the hot storage tank (HST) to the ambient environment, modeled through a global heat transfer coefficient and surface area. During nighttime hours, in the absence of solar input, the thermal losses progressively reduce the tank temperature, allowing the system to approach a quasi-thermodynamic equilibrium before the next operating cycle. It is apparent that in Figure 5a–c, which pertain to pure water and all flow rates, the collectors' outlet temperature stays below 80 °C—the designated temperature set point for the supplementary boiler. Conversely, for Figure 5d–i, as the concentration of nanoparticles in the solution increases, the collectors' outlet temperature exceeds 80 °C for most of the day.

The highest temperature was observed at a volumetric flow rate of 0.24 L/s and a volumetric concentration of 0.6%, as depicted in Figure 5g. This phenomenon can be attributed to two potential factors: the nanofluids exhibit diminished absorption ability at increasing volumetric concentrations, and there is a continual influx of heat. However, while utilizing an Al_2O_3–water nanofluid with a volumetric particle concentration of φ = 0.3%, the temperature remains comparable to that of a nanofluid with a volumetric concentration of φ = 0.6% because of the reduced difference thermal conductivity of the fluid. The outlet temperature of the collectors, in all cases, was consistently higher for Al_2O_3–water nanofluid compared to pure water. The higher outlet temperatures observed

with nanofluids are not only due to enhanced solar heat absorption, but also to their improved thermal conductivity and modified specific heat capacity. These properties contribute to more efficient heat transfer inside the collector tubes and more uniform temperature distribution, resulting in higher thermal energy gain at the collector outlet. The simulation findings indicate a maximum deviation of up to 19% (0.3% vol.) and 33% (0.6% vol.) in the hourly outlet collector temperatures between the configuration using pure water and that using nanofluids, with a flow rate of 0.24 L/s.

The superior thermal behavior observed at 0.6% volume fraction is primarily due to the improved effective thermal conductivity of the nanofluid. Higher nanoparticle concentration increases the surface area available for heat transfer and enhances Brownian motion, which leads to more efficient energy transport within the fluid. Moreover, the reduction in specific heat slightly improves the rate of temperature rise, contributing to earlier achievement of the chiller input setpoint temperature.

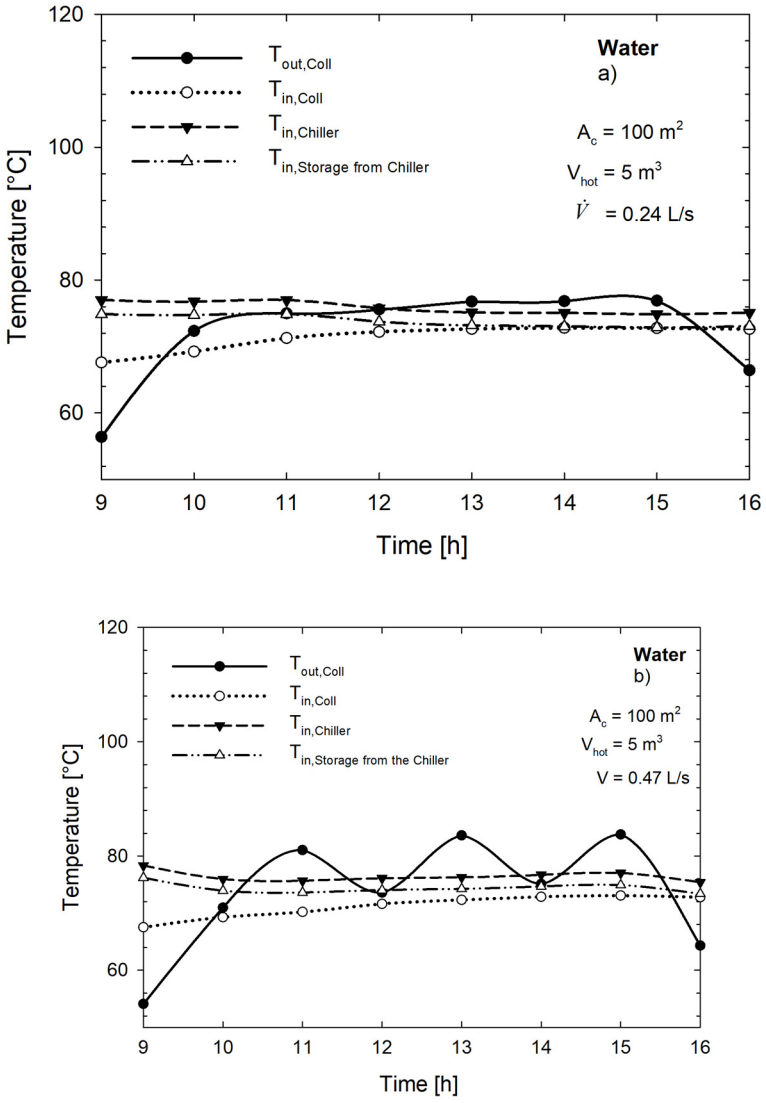

Figure 5. *Cont.*

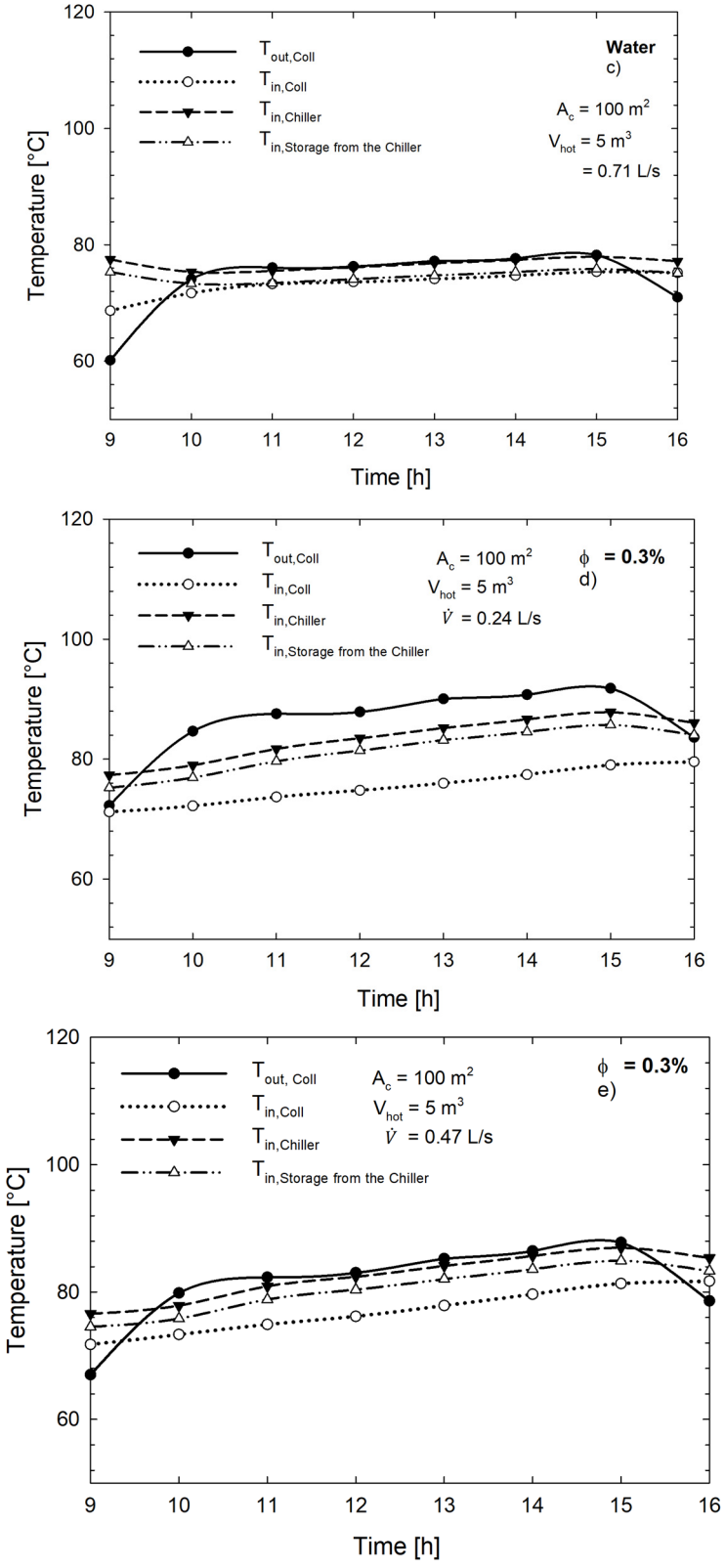

Figure 5. *Cont.*

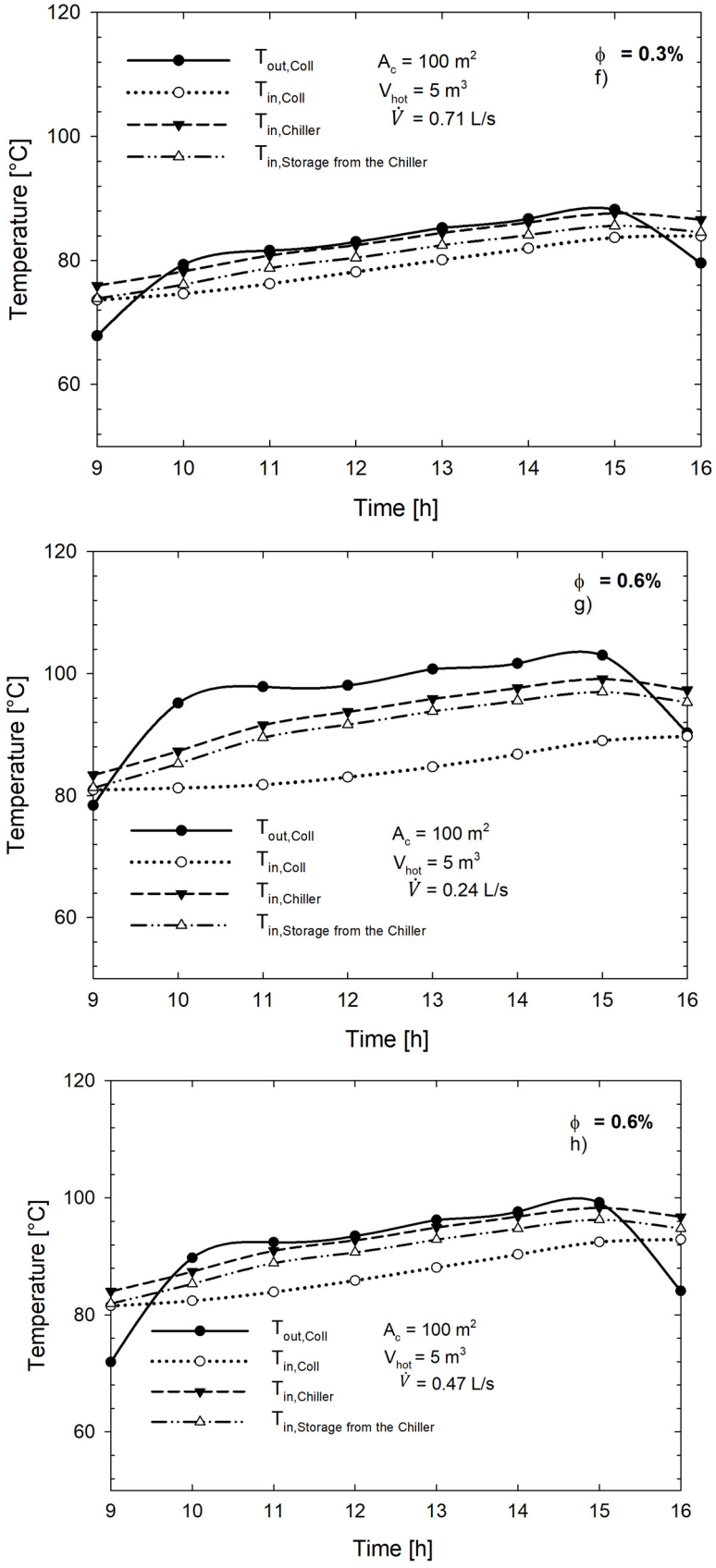

Figure 5. *Cont*.

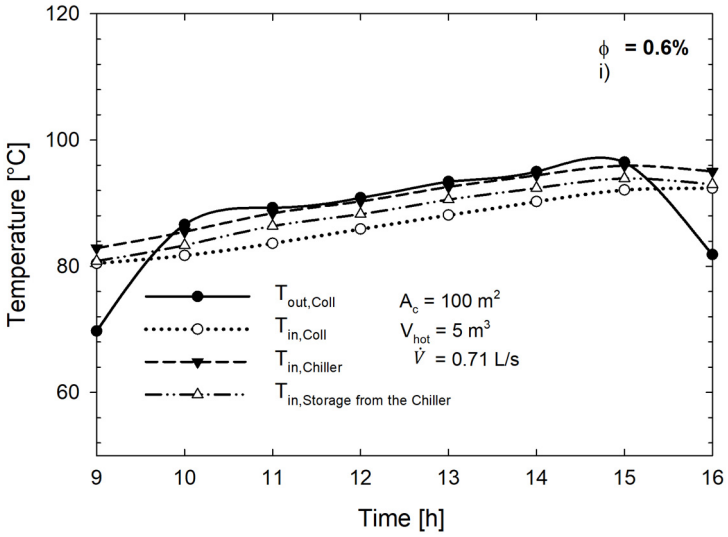

Figure 5. Significant temperature in the solar cooling system. The curves illustrate the outlet temperatures of the collectors and storage tank under various flow rates and nanofluid concentrations: (**a**) water and 0.24 L/s volume flow rate; (**b**) water and 0.47 L/s volume flow rate; (**c**) water and 0.71 L/s volume flow rate; (**d**) 0.3% nanoparticles concentrations and 0.24 L/s; (**e**) 0.3% nanoparticles concentrations and 0.47 L/s; (**f**) 0.3% nanoparticles concentrations and 0.71 L/s; (**g**) 0.6% nanoparticles concentrations and 0.24 L/s; (**h**) 0.6% nanoparticles concentrations and 0.47 L/s; (**i**) 0.6% nanoparticles concentrations and 0.71 L/s.

5.2. Heat Energy

The seasonal variation in the solar collector and auxiliary boiler's heat energy flows is depicted in Figure 6. The key difference between the three different volumetric concentrations is the monthly heat energy of the auxiliary boiler, Q_{boiler}. For pure water, the auxiliary boiler is on for the whole time because the fluid's temperature at the tank outlet, $T_{st,o}$, is lower than 90 °C, while in the configurations with nanofluids, the auxiliary boiler is off for much of the time. In particular, at the highest volumetric concentration of nanoparticles, it can be seen that the monthly energy gain from the solar collector, Q_{solar}, increases while the energy of the auxiliary boiler decreases. In the summertime, the amount of supplementary energy (Q_{boiler}) exceeds the solar thermal gain from the collectors (Q_{solar}) when water is regarded as an auxiliary fluid.

Additionally, the cooling energy requirement is at its peak when there is a substantial disparity between Q_{solar} and Q_{boiler}. The disparity is comparatively reduced during June and September. In June, Q_{solar} is elevated due to low cooling demand, the HST is not influenced by hot water from the absorption chiller, and there is a higher temperature of inlet water into the solar collectors. In September, Q_{solar} and Q_{boiler} reach their lowest points because solar irradiation and cooling demand both decrease. With respect to nanofluids, it is observed that Q_{solar} is consistently higher than Q_{boiler} throughout the summer season. Even during the hottest months, the increased work of the chiller does not lead to a substantial decrease in the temperature of the storage tank. Furthermore, the T_{inlet} of the auxiliary fluid in the solar collectors rises, leading to an increase in solar thermal gain. This effect is even more pronounced when using nanofluids with a volumetric concentration of $\varphi = 0.6\%$. It is worth noting that during warmer months, the supplementary energy required is minimal, allowing the absorption machine to operate solely with the contribution from the solar field.

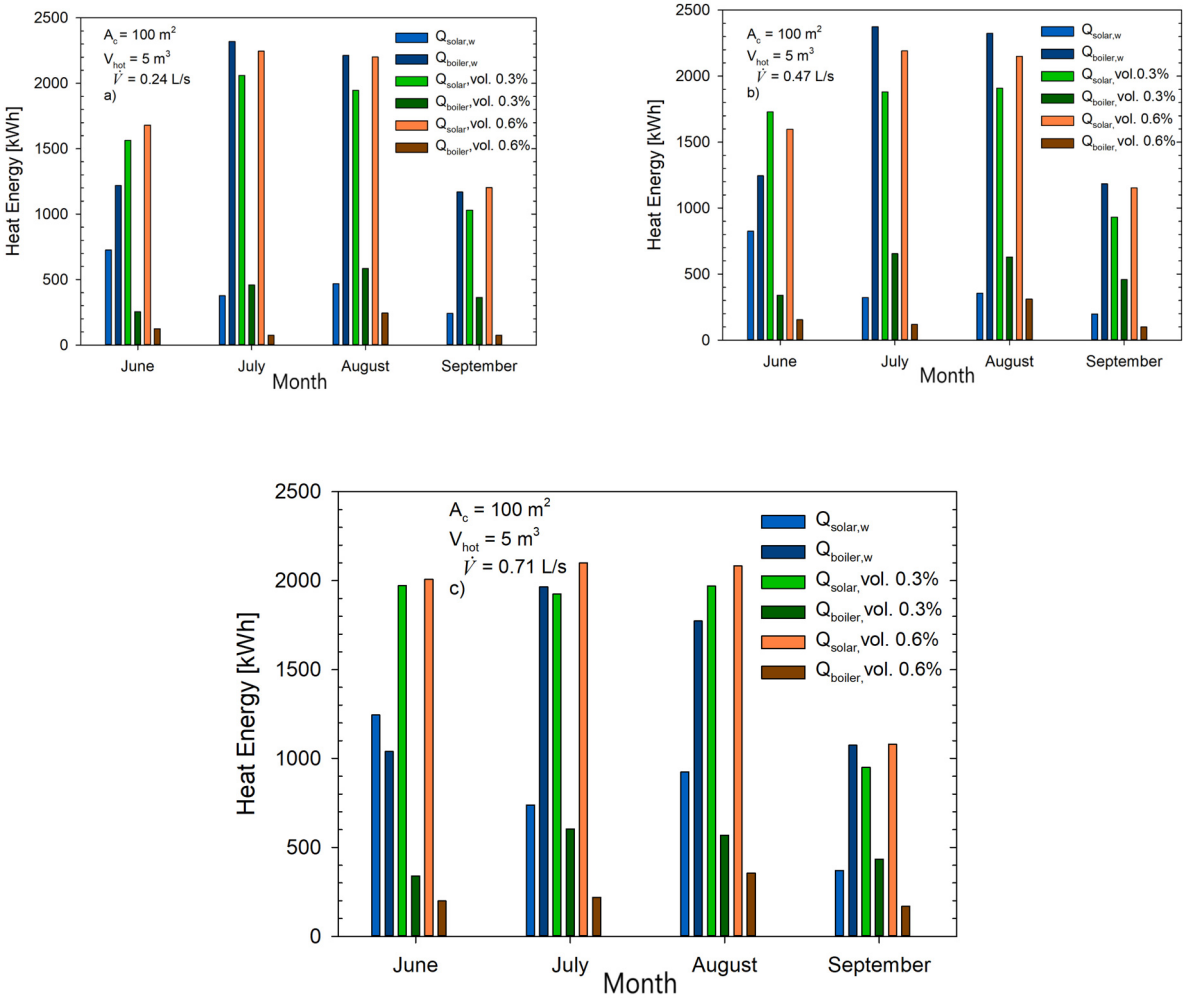

Figure 6. Thermal energy provided by the solar field and auxiliary boiler for different nanofluid concentrations. Results show a significant reduction in boiler energy consumption when using nanofluids, particularly at 0.6% volume: (**a**) volume flow rate equal to 0.24 L/s; (**b**) volume flow rate equal to 0.47; (**c**) volume flow rate equal to 0.71 L/s.

The reduction in Q_{boiler} observed for nanofluid cases is due to the higher outlet temperatures from the solar collectors, which allow the storage tank to remain at or above the chiller's required input temperature for longer periods. This decreases the frequency of auxiliary boiler activation. The enhanced thermal conductivity of nanofluids enables more efficient solar energy absorption and transfer to the storage tank, resulting in more stable and prolonged high-temperature operation.

5.3. Performance Results

Figure 7 illustrates the monthly variations in solar fraction resulting from varying volumetric flow rates and nanoparticle concentrations. The greatest solar fraction is achieved when employing nanofluid with a volumetric concentration of φ = 0.6% across all flow rates examined. In contrast, when pure water is utilized, a decline in SF is evident during warmer months due to heightened influence of $T_{hot,\,out}$ from the absorption chiller. Extended operation of the absorption chiller leads to a decrease in temperature within the Hot Storage Tank (HST), thereby necessitating prolonged use of the auxiliary heater.

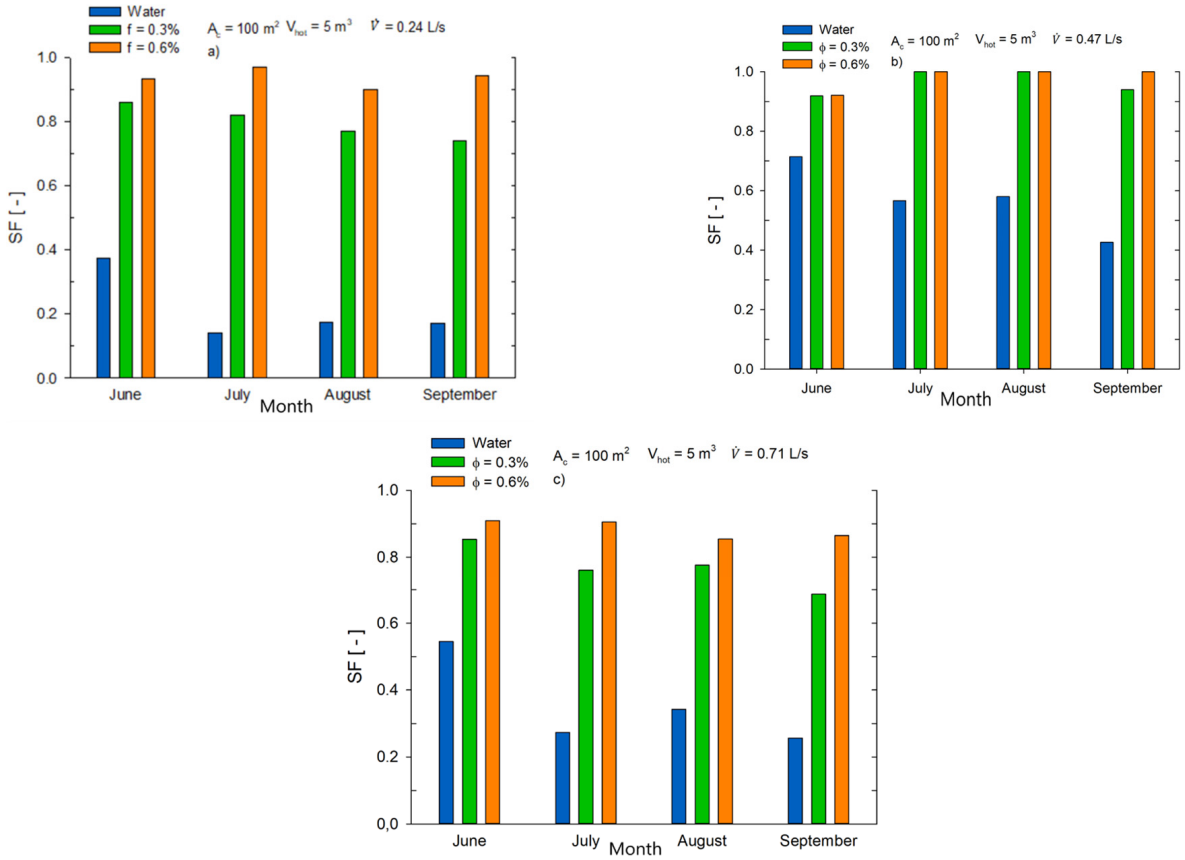

Figure 7. Solar fraction. Nanofluids significantly increase the fraction of energy supplied by the solar field, with SF reaching 1 in some configurations: (**a**) volume flow rate equal to 0.24 L/s; (**b**) volume flow rate equal to 0.47; (**c**) volume flow rate equal to 0.71 L/s.

Moreover, the findings demonstrate that utilizing a mixture of Al_2O_3 and water with a concentration of 0.3% and 0.6%, respectively, results in a significant increase in SF, up to 74.6%, when compared to pure water as a working fluid, particularly for a volumetric flow rate of 0.24 L/s. Therefore, for the reasons previously stated, the optimal performance in terms of solar fractions is achieved at a lower volumetric flow rate.

Figure 8 illustrates the monthly variation in fractional primary energy savings, denoted as f. As the energy demand of the auxiliary heater increases, the primary energy savings diminishes, and conversely, when it decreases, the primary energy savings improves. In instances where the value of f falls below zero, as observed with pure water, it indicates that the solar cooling system may not meet the cooling energy requirements throughout the entire summer season, unlike a conventional compression machine. Additionally, in June and September, despite the lower Q_{boiler} compared to other months, a conventional cooling system consumes more primary energy due to fewer hot days during these months.

During the months of June, July, and August, Q_{boiler} is elevated, but so is the energy consumption of a vapor compression system, resulting in higher values of f during the other months. However, for systems employing nanofluids, the seasonal variation in f decreases at a higher volumetric flow rate, whereas for pure water, it increases.

To assess the feasibility of utilizing nanofluids in collectors in terms of overall primary energy, the energy consumption of the pumping process is also computed and presented in Figure 9. The system that utilizes 0.3% concentration of nanofluid as the auxiliary fluid exhibits higher mechanical energy than the configurations with pure water and 0.6% concentration, across all volumetric flow rates.

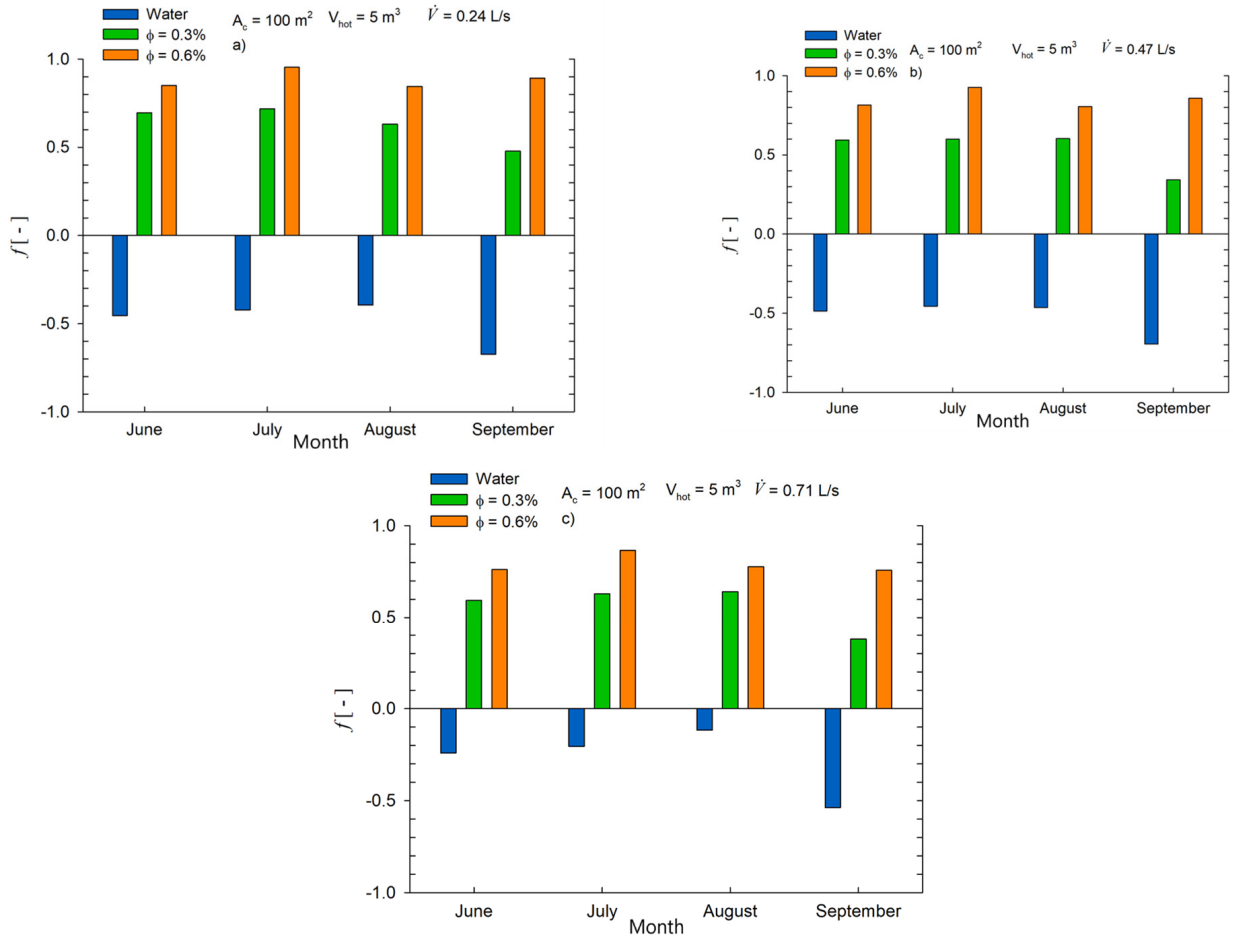

Figure 8. Primary energy savings. The graph shows improved energy savings when using nanofluids, particularly at low flow rates, compared to pure water: (**a**) volume flow rate equal to 0.24 L/s; (**b**) volume flow rate equal to 0.47; (**c**) volume flow rate equal to 0.71 L/s.

The energy required for pumping a nanofluid is greater due to the higher value of viscosity. Additionally, the pumping energy consumption for a concentration of 0.3% is higher than that for 0.6% due to the greater impact of $T_{hot,out}$ from the absorption chiller on the HST temperature, which results in a longer duration of pump operation.

The electrical consumption of the pump was estimated using the Darcy–Weisbach equation [35] to evaluate the pressure drop in the solar loop, considering the dynamic viscosity of the working fluid (which varies with nanofluid concentration). The volumetric flow rate was multiplied by the pressure drop to obtain hydraulic power, which was then divided by a typical pump efficiency (assumed to be 60%) to obtain the electric energy required. Head losses were considered in terms of pipe length, diameter, and minor losses due to fittings. As nanoparticle concentration increases from 0.3% to 0.6%, the viscosity increases by approximately 8%, resulting in a pumping energy increase of up to 5% at the highest flow rate (0.71 L/s). This trade-off was included in the energy balance and supports the importance of optimizing both thermal and hydraulic performance. A sensitivity analysis confirmed that viscosity has a moderate influence on the solar fraction (see Table 6). The examination of the amount of energy used for pumping shows that nanofluids are the most favorable option when considering the same amount of fluid flow, since the difference in energy cost is very small in percentage terms as defined in Table 7. All values reported in Table 6 refer to cumulative results over a four-month simulation period, from June to September, representing the entire cooling season.

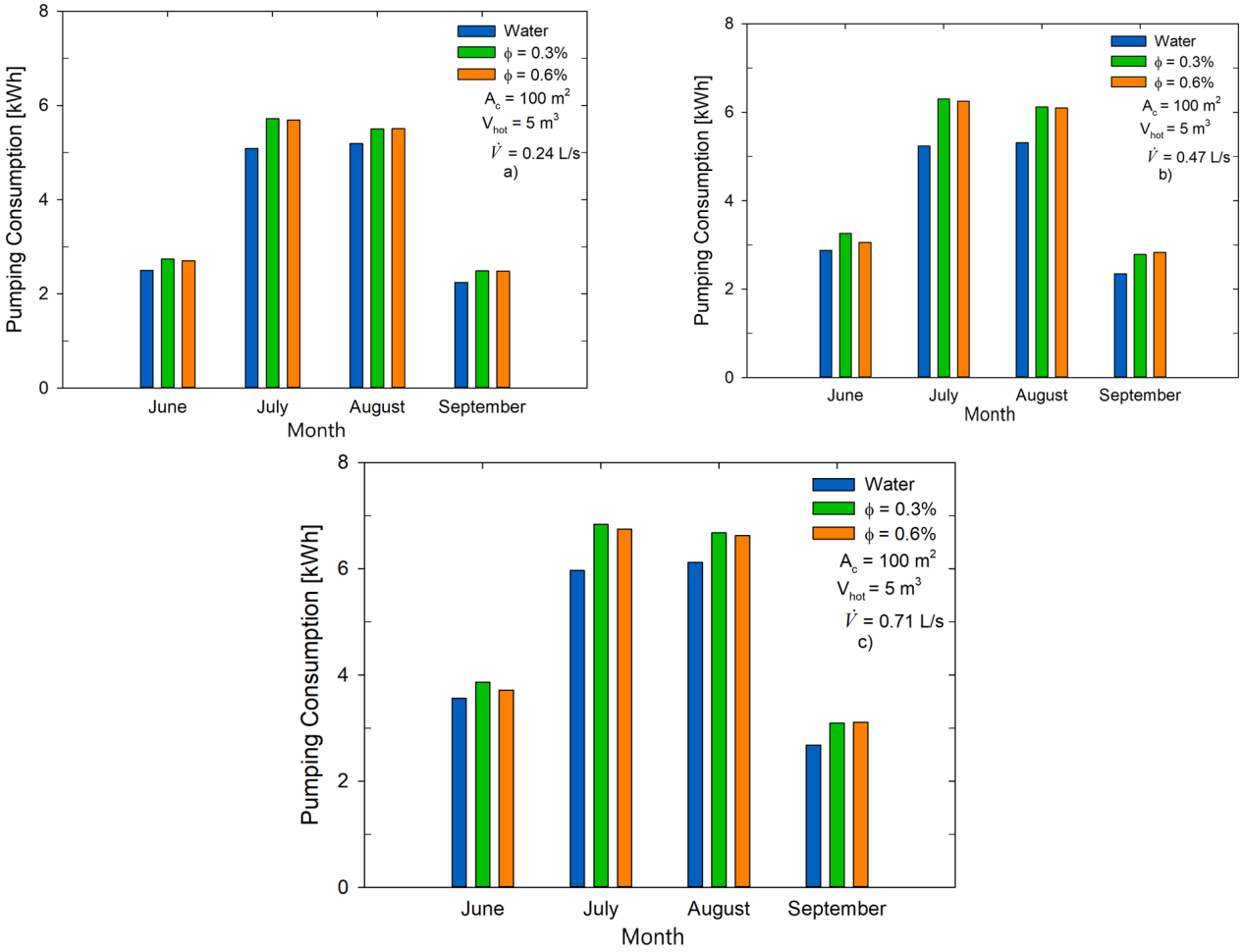

Figure 9. Pumping consumption. Despite slightly higher viscosity, nanofluids result in modest increases in pumping energy, which are offset by significant gains in solar efficiency: (**a**) volume flow rate equal to 0.24 L/s; (**b**) volume flow rate equal to 0.47; (**c**) volume flow rate equal to 0.71 L/s.

Table 7. Percentage improvements of the more significant parameters by using nanofluids as working fluid into ETSCs.

Results	$\dot{V}$ **= 0.24 L s^{-1}**		$\dot{V}$ **= 0.47 L s^{-1}**		$\dot{V}$ **= 0.47 L s^{-1}**	
	0.3% vol.	**0.6% vol.**	**0.3% vol.**	**0.6% vol.**	**0.3% vol.**	**0.6% vol.**
Temperature						
Collector outlet temperatureSu	19.88%	33.06%	11.88%	24.37%	10.34%	18.89%
Collector inlet temperature	5.70%	18.56%	8.23%	22.43%	7.75%	18.33%
Storage outlet temperature	10.07%	23.07%	7.98%	21.42%	7.98%	18.13%
Energy						
Solar gain from collectors	300.69%	348.18%	349.28%	414.13%	478.80%	503.67%
Supplementary boiler	−75.44%	−92.27%	−69.83%	−90.19%	−66.02%	−83.46%
Pumping consumption	9.74%	9.20%	16.89%	15.29%	11.90%	10.35%

While this study demonstrates the energetic benefits of nanofluids in solar cooling systems, a comprehensive Life Cycle Cost (LCC) analysis was not included. Additionally, long-term performance factors such as nanoparticle sedimentation, stability, and material compatibility require further investigation. Future work will focus on integrating techno-economic analysis and experimental validation to assess system durability and real-world applicability.

Overall, the use of Al_2O_3–water nanofluids in the solar loop leads to significant enhancements in thermal performance across multiple indicators: collector outlet temperature, solar fraction, and primary energy savings. These improvements confirm the potential of nanofluids as a viable strategy for increasing the efficiency of solar cooling systems under realistic climatic conditions, particularly when operating at low to medium flow rates. Additionally, the moderate increase in pumping energy is negligible compared to the thermal performance gains, reinforcing the practicality of implementing such fluids in real-world installations.

6. Conclusions

This study investigated the impact of using Al_2O_3–water nanofluids in the solar loop of a dynamic solar-assisted absorption cooling system, with simulations performed under realistic operating conditions for a Mediterranean climate. Based on the results, the main conclusions are:

- Enhanced Thermal Performance: The use of nanofluids led to significantly higher outlet temperatures from the solar collectors compared to pure water, due to improved thermal conductivity and heat transfer characteristics.
- Increased Solar Fraction: A solar fraction (SF) close to or equal to 1 was achieved in several configurations using nanofluids, especially at low volumetric flow rates, demonstrating a substantial reduction in reliance on auxiliary energy sources.
- Higher Primary Energy Savings: Configurations with nanofluids, particularly at 0.6% concentration, yielded seasonal primary energy savings exceeding 80%, highlighting the effectiveness of nanofluids in improving overall system efficiency.
- Acceptable Pumping Penalty: Although nanofluids increase the dynamic viscosity, the associated increase in pumping energy was modest (below 5%) and largely offset by thermal efficiency gains.
- Practical Applicability: The use of nanofluids in the solar loop only, combined with a realistic system layout and operating conditions, confirms their feasibility for real-world solar cooling installations.
- Future developments will include full-year simulations and the integration of techno-economic and life-cycle analyses to support broader deployment of nanofluid-enhanced solar thermal systems.

Author Contributions: Conceptualization, L.C., S.G., A.G., C.M., S.N., V.O. and L.V.; Methodology, L.C., A.G., C.M., S.N., V.O. and L.V.; Software, L.C., A.G., C.M., S.N., V.O. and L.V.; Validation, L.C., A.G., C.M., S.N. and L.V.; Formal analysis, L.C., A.G., C.M., S.N. and L.V.; Investigation, L.C., S.G., A.G., C.M., S.N., V.O. and L.V.; Resources, L.C., A.G., C.M. and S.N.; Data curation, L.C., A.G., C.M. and S.N.; Writing—original draft, L.C., S.G., A.G., C.M., S.N., V.O. and L.V.; Writing—review & editing, L.C. and S.N.; Visualization, L.C., S.G., A.G., C.M., S.N. and L.V.; Supervision, L.C. and S.N.; Project administration, L.C. and S.N.; Funding acquisition, L.C. and S.N. All authors have read and agreed to the published version of the manuscript.

Funding: This research did not receive any specific grant from funding agencies in the public, commercial, or not-for-profit sectors.

Data Availability Statement: The original contributions presented in the study are included in the article, further inquiries can be directed to the corresponding author.

Conflicts of Interest: The authors declare no conflict of interest.

Nomenclature

A_c	Solar collector area (m^2)
B	Boiler (-)
C	Controller (-)
CH	Chiller (-)
COP	Coefficient of performance (-)
CST	Cold storage tank (-)
CT	Cooling tower (-)
c_p	Specific heat (J kg^{-1} K^{-1})
DW	Distilled water (-)
ETCs	Evacuated tube solar collectors (-)
FC	Fan coil (-)
FPC	Flat plate solar collector (-)
HST	Hot storage tank (-)
k	Thermal conductivity (Wm^{-1} K^{-1})
f	Fractional primary energy saving for a solar cooling system (-)
G	Incident global solar radiation on the collector (W m^{-2})
P	Pump (-)
Q_{boiler}	Heat energy of the auxiliary boiler (kWh)
Q_{solar}	Heat energy gain from solar collectors (kWh)
$Q_{cooling,ref}$	Energy cold provided by a conventional system (kWh)
SCS	Solar cooling system (-)
SF	Solar fraction (-)
$T_{coll,o}$	Outlet temperature of solar collector (°C)
$T_{coll,i}$	Inlet temperature of solar collector (°C)
$T_{st,i}$	Inlet temperature of hot storage tank (°C)
$T_{st,o}$	Outlet temperature of hot storage tank (°C)
$\dot{V}$	Volumetric flow rate (l s^{-1})
Vol	Volumetric concentration (%)
Greek symbols	
η	Thermal efficiency of solar collector (-)
ε_{heat}	Efficiency of supplementary boiler (-)
$\varepsilon_{cooling}$	Efficiency of thermal power plant (-)
ϕ	Solid volume fraction (%)
ρ	Density (kg m^{-3})
μ	Dynamic viscosity (kg $m^{-1}s^{-1}$)
ΔT	Temperature difference between fluid and ambient temperature (°C)
Subscripts	
bf	Base fluid (water)
p	Nanoparticle
w	Water
nf	Nanofluid

References

1. Xuan, Y.; Li, Q. Heat transfer enhancement of nanofluids. *Int. J. Heat Fluid Flow* **2000**, *21*, 58–64. [CrossRef]
2. Choi, S.U.; Eastman, J.A. Enhancing thermal conductivity of fluids with nanoparticles. In *ASME International Mechanical Engineering Congress & Exposition*; Argonne National Lab: Argonne, IL, USA, 1995.
3. Almanassra, I.W.; Manasrah, A.D.; Al-Mubaiyedh, U.A.; Al-Ansari, T.; Malaibari, Z.O.; Atieh, M.A. An experimental study on stability and thermal conductivity of water/CNTs nanofluids using different surfactants: A comparison study. *J. Mol. Liq.* **2020**, *304*, 111025. [CrossRef]
4. Karakaş, A.; Harikrishnan, S.; Öztop, H.F. Preparation of EG/water mixture-based nanofluids using metal-oxide nanocomposite and measurement of their thermophysical properties. *Therm. Sci. Eng. Prog.* **2022**, *36*, 101538. [CrossRef]

5. Ju, X.; Liu, H.; Pei, M.; Li, W.; Lin, J.; Liu, D.; Ju, X.; Xu, C. Multi-parameter study and genetic algorithm integrated optimization for a nanofluid-based photovoltaic/thermal system. *Energy* **2023**, *267*, 126528. [CrossRef]
6. Lin, H.; Jian, Q.; Bai, X.; Li, D.; Huang, Z.; Huang, W.; Feng, S.; Cheng, Z. Recent advances in thermal conductivity and thermal applications of graphene and its derivatives nanofluids. *Appl. Therm. Eng.* **2023**, *218*, 119176. [CrossRef]
7. Alktranee, M.; Shehab, M.A.; Németh, Z.; Bencs, P.; Hernadi, K. Effect of zirconium oxide nanofluid on the behaviour of photovoltaic–thermal system: An experimental study. *Energy Rep.* **2023**, *9*, 1265–1277. [CrossRef]
8. Das, L.; Aslfattahi, N.; Habib, K.; Saidur, R.; Irshad, K.; Yahya, S.M.; Kadirgama, K. Improved thermophysical characteristics of a new class of ionic liquid + diethylene glycol/Al_2O_3 + CuO based ionanofluid as a coolant media for hybrid PV/T system. *Therm. Sci. Eng. Prog.* **2022**, *36*, 101518. [CrossRef]
9. Sarchami, A.; Tousi, M.; Kiani, M.; Arshadi, A.; Najafi, M.; Darab, M.; Houshfar, E. A novel nanofluid cooling system for modular lithium-ion battery thermal management based on wavy/stair channels. *Int. J. Therm. Sci.* **2022**, *182*, 107823. [CrossRef]
10. Chinchole, A.S.; Dasgupta, A.; Kulkarni, P.P.; Chandraker, D.K.; Nayak, A.K. Exploring the Use of Alumina Nanofluid as Emergency Coolant for Nuclear Fuel Bundle. *J. Therm. Sci. Eng. Appl.* **2019**, *11*, 021007. [CrossRef]
11. El Kholy, A.; Alyan, A.; Fakhry, K.; Abu-Elyazeed, O. Thermal hydraulic analysis of supercritical water reactor cooled by TiO_2 nanofluid. *J. Nucl. Sci. Technol.* **2019**, *56*, 291–299. [CrossRef]
12. Mostafizur, R.; Rasul, M.; Nabi, M.; Saianand, G. Properties of Al_2O_3-MWCNT/radiator coolant hybrid nanofluid for solar energy applications. *Energy Rep.* **2022**, *8*, 582–591. [CrossRef]
13. Elshazly, E.; Abdel-Rehim, A.A.; El-Mahallawi, I. Thermal performance enhancement of evacuated tube solar collector using MWCNT, Al_2O_3, and hybrid MWCNT/Al_2O_3nanofluids. *Int. J. Thermofluids* **2023**, *17*, 100260. [CrossRef]
14. Azeez, K.; Abu Talib, A.R.; Ibraheem Ahmed, R. Heat transfer enhancement for corrugated facing step channels using aluminium nitride nanofluid-numerical investigation. *J. Therm. Eng.* **2022**, *8*, 734–747. [CrossRef]
15. Uniyal, A.; Prajapati, Y.K.; Ranakoti, L.; Bhandari, P.; Singh, T.; Gangil, B.; Sharma, S.; Upadhyay, V.V.; Eldin, S.M. Recent Advancements in Evacuated Tube Solar Water Heaters: A Critical Review of the Integration of Phase Change Materials and Nanofluids with ETCs. *Energies* **2022**, *15*, 8999. [CrossRef]
16. Greco, A.; Gundabattini, E.; Gnanaraj, D.S.; Masselli, C. A comparative study on the performances of flat plate and evacuated tube collectors deployable in domestic solar water heating systems in different climate areas. *Climate* **2020**, *8*, 78. [CrossRef]
17. Cirillo, L.; Della Corte, A.; Nardini, S. Feasibility study of solar cooling thermally driven system configurations for an office building in mediterranean area. *Int. J. Heat Technol.* **2016**, *34*, S472–S480. [CrossRef]
18. Cascetta, F.; Di Lorenzo, R.; Nardini, S.; Cirillo, L. A Trnsys Simulation of a Solar-Driven Air Refrigerating System for a Low-Temperature Room of an Agro-Industry site in the Southern part of Italy. *Energy Procedia* **2017**, *126*, 329–336. [CrossRef]
19. Hawwash, A.; Rahman, A.K.A.; Nada, S.; Ookawara, S. Numerical Investigation and Experimental Verification of Performance Enhancement of Flat Plate Solar Collector Using Nanofluids. *Appl. Therm. Eng.* **2018**, *130*, 363–374. [CrossRef]
20. Eyyamoglu, B.; Bahlouli, K. Performance and economic analysis of a nanofluid-based solar-driven trigeneration system for a residential building in Cyprus. *Appl. Therm. Eng.* **2025**, *277*, 127001. [CrossRef]
21. Shaalan, Z.A.; Hussein, A.M.; Abdullah, M.Z.; Alsayah, A.M.; Alshukri, M.J.; Khaled, M. Enhanced photovoltaic cooling using ZnO/TiO_2 hybrid nanofluids: Numerical and experimental analysis. *Int. J. Thermofluids* **2025**, *27*, 101222. [CrossRef]
22. Aissa, A.; Qasem, N.A.; Mourad, A.; Laidoudi, H.; Younis, O.; Guedri, K.; Alazzam, A. A review of the enhancement of solar thermal collectors using nanofluids and turbulators. *Appl. Therm. Eng.* **2023**, *220*, 119663. [CrossRef]
23. Muhammad, M.J.; Muhammad, I.A.; Sidik, N.A.C.; Yazid, M.N.A.W.M. Thermal performance enhancement of flat-plate and evacuated tube solar collectors using nanofluid: A review. *Int. Commun. Heat Mass Transf.* **2016**, *76*, 6–15. [CrossRef]
24. Cascetta, F.; Cirillo, L.; Nardini, S.; Vigna, S. Transient Simulation of a Solar Cooling System for an Agro-Industrial Application. *Energy Procedia* **2018**, *148*, 328–335. [CrossRef]
25. Buonomo, B.; Cascetta, F.; Cirillo, L.; Nardini, S. Application of nanofluids in solar cooling system: Dynamic simulation by means of TRNSYS software. *Model. Meas. Control B* **2018**, *87*, 143–150. [CrossRef]
26. Xuan, Y.; Roetzel, W. Conceptions for heat transfer correlation of nanofluids. *Int. J. Heat Mass Transf.* **2000**, *43*, 3701–3707. [CrossRef]
27. Ghaderian, J.; Sidik, N.A.C. An experimental investigation on the effect of Al_2O_3/distilled water nanofluid on the energy efficiency of evacuated tube solar collector. *Int. J. Heat Mass Transf.* **2017**, *108*, 972–987. [CrossRef]
28. Kasaeian, A.; Daneshazarian, R.; Pourfayaz, F. Comparative study of different nanofluids applied in a trough collector with glass-glass absorber tube. *J. Mol. Liq.* **2017**, *234*, 315–323. [CrossRef]
29. Sarkar, J. A critical review on convective heat transfer correlations of nanofluids. *Renew. Sustain. Energy Rev.* **2011**, *15*, 3271–3277. [CrossRef]
30. Khan, S.M.A.; Badar, A.W.; Siddiqui, M.S.; Siddique, M.Z.; Ul Haq, M.S.; Butt, F.S. Modeling and comparative assessment of solar thermal systems for space and water heating: Liquid water versus air-based systems. *J. Renew. Sustain. Energy* **2023**, *15*, 063702. [CrossRef]

31. Available online: https://maya-airconditioning.com/assorbitori-ad-acqua/ (accessed on 5 June 2025).
32. Shirazi, A.; Taylor, R.A.; Morrison, G.L.; White, S.D. A comprehensive, multi-objective optimization of solar-powered absorption chiller systems for air-conditioning applications. *Energy Convers. Manag.* **2017**, *132*, 281–306. [CrossRef]
33. Fong, K.F.; Chow, T.T.; Lee, C.K.; Lin, Z.; Chan, L.S. Comparative study of different solar cooling systems for buildings in subtropical city. *Sol. Energy* **2010**, *84*, 227–244. [CrossRef]
34. Sparber, W.; Thuer, A.; Besana, F.; Streicher, W.; Henning, H.M. Unified Monitoring Procedure and Performance Assessment for Solar Assisted Heating and Cooling Systems. In Proceedings of the 1st International Conference on Solar Heating, Cooling and Buildings, Lisbon, Portugal, 7–10 October 2008.
35. White, F.M. *Fluid Mechanics*, 8th ed.; McGraw-Hill Education: New York, NY, USA, 2016.